Revisiting Whitlockite, the Second Most Abundant Biomineral in Bone: Nanocrystal Synthesis in Physiologically Relevant Conditions and Biocompatibility Evaluation

Hae Lin Jang,[†] Kyoungsuk Jin,[†] Jaehun Lee,[†] Younghye Kim,[†] Seung Hoon Nahm,[‡] Kug Sun Hong,[†] and Ki Tae Nam[†,*]

[†]Department of Materials Science and Engineering, Seoul National University, Seoul, 151-744, Korea and [‡]Korea Research Institute of Standards and Science, Daejeon 305-340, Korea

ABSTRACT The synthesis of pure whitlockite (WH: $Ca_{18}Mg_2(HPO_4)_2(PO_4)_{12}$) has remained a challenge even though it is the second most abundant inorganic in living bone. Although a few reports about the precipitation of WH in heterogeneous phases have been published, to date, synthesizing WH without utilizing any effects of a buffer or various other ions remains difficult. Thus, the related research fields have encountered difficulties and have not been fully developed. Here, we developed a large-scale synthesis method for pure WH nanoparticles in a ternary $Ca(OH)_2$—$Mg(OH)_2$—H_3PO_4 system based on a systematic approach. We used excess Mg^{2+} to impede the growth of hydroxyapatite (HAP: $Ca_{10}(PO_4)_6(OH)_2$) and the formation of other kinetically favored calcium phosphate intermediate phases. In addition, we designed and investigated the synthesis conditions of WH under the acidic pH conditions required to dissolve HAP, which is the most thermodynamically stable phase above pH 4.2, and to incorporate the HPO_4^{2-} group into the chemical structure of WH. We demonstrated that pure WH nanoparticles can be precipitated under Mg^{2+}-rich and acidic pH conditions without any intermediate phases. Interestingly, this synthesized nano-WH showed comparable biocompatibility with HAP. Our methodology for determining the synthesis conditions of WH could provide a new platform for investigating other important precipitants in aqueous systems.

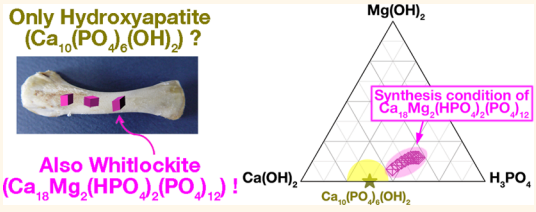

KEYWORDS: biomineralization · bone growth · whitlockite · nanoparticle · calcium phosphate · inorganic synthesis · biomaterial

Whitlockite (WH: $Ca_{18}Mg_2(HPO_4)_2(PO_4)_{12}$) is one of the main components of hard tissue in living creatures;[1−6] however, its importance and role have not been fully identified. While bone acts as a storehouse for 99% of the Ca^{2+} and more than 50% of the Mg^{2+} in our body,[2,7] the majority mineral is hydroxyapatite (HAP: $Ca_{10}(PO_4)_6(OH)_2$),[8−10] which almost cannot incorporate Mg^{2+} in its lattice structure.[2,11] The WH proportion may be estimated to be approximately 20% in bone mineral based on the amount of Mg^{2+}.[2] In addition, dentin can contain approximately 26% to 58% WH by weight.[2] Notably, the ratio of WH to HAP is higher in younger individuals[12] and during the earlier stages of mineralization.[13] However, currently, very little is known about WH in terms of its mechanism of formation or contribution in our body. The basic reason for this mystery is that detecting WH in our body is difficult because it exists locally only over a short-range. Another reason is that synthesizing a pure phase of WH in an aqueous-based physiological system is also difficult. Thus, despite the significant amount of WH in our body, related fields have encountered difficulties in investigations. Biologically existing WH has never been implemented in a clinical trial, whereas the synthetic analogue tricalcium phosphate (TCP, $Ca_3(PO_4)_2$) has been widely used in implants and cell-culturing scaffolds.

WH is a biologically important phase in bone but is difficult to synthesize, most likely because it is thermodynamically

* Address correspondence to nkitae@snu.ac.kr.

Received for review October 8, 2013 and accepted December 3, 2013.

Published online December 03, 2013
10.1021/nn405246h

stable over a narrow region. It has been long hypothesized that WH can be formed in slight preference to the well-known intermediate dicalcium phosphate dehydrate (DCPD: $CaHPO_4 \cdot 2H_2O$) or defective hydroxyapatite (DHA: $Ca_9(HPO_4)(PO_4)_5(OH)$) only between pH 7 and pH 8 but transforms into HAP, which is the most stable calcium phosphate crystal, above pH 4.2.[14] This long-conceived prediction is based on the estimation of the ion activity product from a compositional analysis of the precipitates. However, only a few studies have been conducted to further understand the formation mechanism and to identify the stabilizing conditions of WH. The experimental difficulty is mainly due to the existence of too many intermediate phases, including DCPD, octacalcium phosphate (OCP: $Ca_8(HPO_4)_2(PO_4)_4 \cdot 5H_2O$), and dicalcium phosphate anhydrous (DCPA: $CaHPO_4$), which eventually transform into HAP near pH 7.

Previously, there have been only limited reports about obtaining the WH phase from aqueous solutions.[1,2,15−17] Rowles simultaneously mixed $CaCl_2$, $MgCl_2$, and Na_2HPO_4 in water at 100 °C to prepare WH.[18] WH has also been prepared by the dropwise addition of a solution containing Ca^{2+} and Mg^{2+} ions into a phosphate solution.[15,19] However, both methods suffered from the formation of other heterogeneous phases, such as HAP and various amorphous secondary phases, which affected the overall crystallinity. WH has also been prepared by Rogez *et al.* using $Ca(NO_3)_2$, $Mg(NO_3)_2$, and $(NH_4)_2HPO_4$.[17] In this study, we designed and presented a simple synthesis of WH in a ternary $Ca(OH)_2-Mg(OH)_2-H_3PO_4$ system, without any other secondary ion or buffer effect. The entire process was conducted in an aqueous system and was always maintained below 100 °C.

RESULTS AND DISCUSSION

To determine the appropriate synthesis conditions for WH, we organized a ternary diagram with the possible precipitants resulting from $Ca(OH)_2$, $Mg(OH)_2$, and H_3PO_4 at 80 °C, as illustrated in Figure 1. In the $Ca(OH)_2-H_3PO_4$ binary system, HAP, DCPA, and MCPM are precipitated based on their composition ratio in the chemical formula. In the $Mg(OH)_2-H_3PO_4$ binary system, dimagnesium phosphate (MP), monomagnesium phosphate (MMP), and trimagneium phosphate (TMP) can be synthesized following their chemical formula. However, we observed that WH could not be precipitated under the stoichiometric conditions of its product (★ in Figure 1). Instead, the majority product formed under these conditions was HAP, as HAP is the most thermodynamically stable phase near neutral pH[14] and is a nonstoichiometric compound that can adopt a wide range of atomic disorders due to its flexible framework.[20] Therefore, the location of the theoretical composition of WH is in a region with a strong preference for HAP precipitation, and thus,

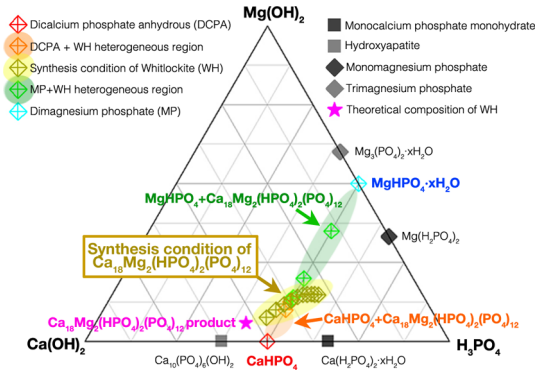

Figure 1. Ternary diagram of precipitants in a $Ca(OH)_2-Mg(OH)_2-H_3PO_4$ aqueous system after 24 h of aging at 80 °C. The newly discovered synthesis conditions of whitlockite examined in this work (gold diamond) and its theoretical composition (magenta star) are indicated. Other closely located calcium phosphate precipitants and magnesium phosphate precipitants are also indicated.

synthesizing WH in the $Ca(OH)_2-Mg(OH)_2-H_3PO_4$ ternary system appeared difficult.

To determine the precipitation conditions for WH and to learn from the previously made TCP, we first analyzed how the phase stability of TCP changes depending on the Mg content and pH. We learned from many previous studies that Mg substitution in TCP (TCMP) stabilizes the phase at low pH compared with pure TCP.[2,21] A detailed example of the activity diagram for the $Ca(OH)_2-Mg(OH)_2-H_3PO_4$ system at 25 °C indicated that TCMP drastically decreased its solubility compared with TCP and even more than HAP. However, Mg^{2+} is known to inhibit HAP[2,18,22] and other kinetically favored intermediate phases of calcium phosphate compounds, such as DCPD,[2,23] DCPA,[2,24] and OCP.[2,25] This fact could suggest a hypothesis that WH is stable under acidic conditions. Because the atomic arrangement in the unit cell is similar for WH and TCP, we hypothesized that the substitution of Mg^{2+} could result in a similar contribution to its stability under acidic conditions.

As illustrated in Figure 2, TCP and TCMP are very closely related to WH. We show the basic unit cell structure of WH with lattice parameters $a = 10.35$ Å and $c = 37.085$ Å in Figure 2a. In the z-axis direction, we observe that WH is composed of two types of columns that are periodically arrayed. In each column, Ca^{2+} ions and PO_4^{3-} ions are regularly arrayed. The B column remains the same in TCP and WH structure compounds, while the differences usually occur in the A column. For example, when Mg^{2+} is incorporated in the TCP structure and produces the TCMP structure, Mg^{2+} substitutes into the previous Ca5 position, as illustrated in Figure 2b. After the Ca5 position is fully substituted with Mg^{2+}, the Ca4 position can also be substituted with Mg^{2+}. For the WH compound, HPO_4^{2-} is also incorporated together with Mg^{2+}

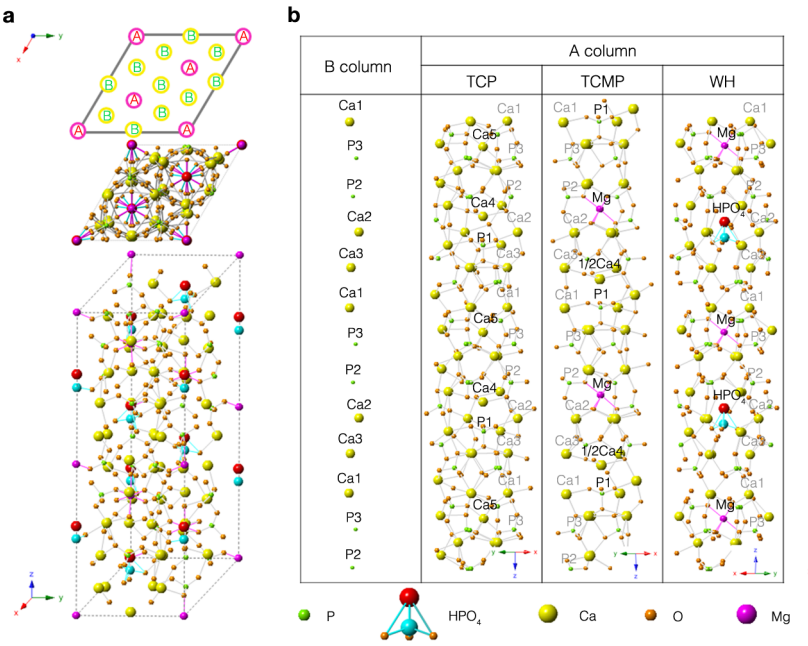

Figure 2. (a) Unit cell of whitlockite (WH) and its $x-y$ plane view from the z-axis direction. Looking down from the z-axis, the A and B columns are periodically arranged in the unit cell of WH. (b) Comparison of the differences in the A column among tricalcium phosphate (TCP), magnesium-substituted tricalcium phosphate (TCMP), and WH; all three compounds have the same atomic arrangement in the B column. The variations in the A column were induced by the incorporation of Mg^{2+} and HPO_4^{2-}. The sizes of main atoms have been exaggerated for easier comparison.

into the A column and forms a crystal structure that is stable enough to be precipitated without requiring a high-temperature sintering process. In addition, TCP and WH also have similar XRD patterns based on rhombohedral crystal structures, and their ratios between cations and anions are similar. Thus, several researchers have previously been confused in distinguishing TCP and WH and have used these terms interchangeably.

It is true that TCP and WH are closely related; however, we can clearly distinguish them by the stable region of their phases and the existence of HPO_4^{2-} in their structure. TCP is a high-temperature phase that cannot be produced in our 37 °C bodies. In addition, TCP cannot avoid transforming into a heterogeneous bulk state after heat treatment. In contrast, WH exists in biological systems and can also be synthesized as nanoparticles below the boiling temperature of water. In addition, we can easily distinguish WH from TCP by detecting the HPO_4^{2-} bond using FT-IR. During heat treatment, a decrease in the weight of WH can also be observed due to the dehydration of HPO_4^{2-} in its structure. Then, notably, WH can transform into the TCMP structure after losing its HPO_4^{2-} group at high temperature.[2,26−28]

As further rationale to design the experimental conditions, we paid attention to the fact that WH contains HPO_4^{2-} together with PO_4^{3-} in its unit cell, which is a notable difference from HAP, which contains PO_4^{3-} only in its theoretical chemical formula. This difference could provide additional evidence that WH can be precipitated at low pH.

Therefore, for our systematic approach, we selected the binary system of $CaHPO_4$ and $MgHPO_4$. Both compounds contain HPO_4^{2-} as an anion and are known to be precipitated more favorably than HAP. Along the compositional line of 50 at. % H_3PO_4, the atomic percentage of Mg in the total cation (Mg + Ca) was varied from 0 to 20%, 40%, 70%, and 100%. The (Mg + Ca):PO_4 ratio was fixed at 1:1, and only the Mg:Ca ratio was varied. $Ca(OH)_2$ powder and $Mg(OH)_2$ powder were dissolved at the various ratios in 500 mL of aqueous solution at 80 °C. The total mole concentration of the cation was fixed at 0.5 M. Then, 500 mL of 0.5 M H_3PO_4 was added dropwise to the 500 mL of $Ca(OH)_2$ and $Mg(OH)_2$ solution at a rate of 12.5 mL/min. Thus, the final ratio of Mg:Ca:P was equal to x:(0.5 − x):0.5 (x = 0, 0.1, 0.2, 0.35, 0.5). After 24 h of incubation under vigorous stirring, the precipitants were collected with a filter press and dried using a lyophilizer for further characterization.

XRD analysis was performed to identify the crystal structure of the precipitants. At x = 0, pure $CaHPO_4$ was precipitated without any minor phase. Notably, at x = 0.1, a minor peak that corresponded to WH started to be observed in addition to the major $CaHPO_4$ peaks. At x = 0.2, the $CaHPO_4$ peak disappeared and instead the $MgHPO_4$ peak appeared along with the WH peak. As x increase to 0.35, the intensity of $MgHPO_4$ increased and that of WH decreased, indicating that the ratio of

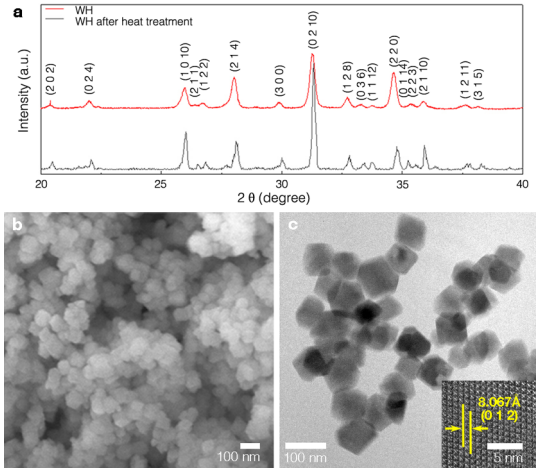

Figure 3. (a) XRD patterns showing the pure phase of the synthesized whitlockite (WH: red line). WH maintained its pure phase even after being heat-treated at 1450 °C for 2 h (gray line). (b) FESEM image of homogeneously formed WH nanoparticles. (c) High-resolution TEM image of rhombohedral shape of WH nanoparticles with approximately 50 nm size. As shown in the bottom right inset, the *d*-spacing value was measured to be 8.067 Å for the WH nanoparticles, which corresponded to the (0 1 2) plane of WH.

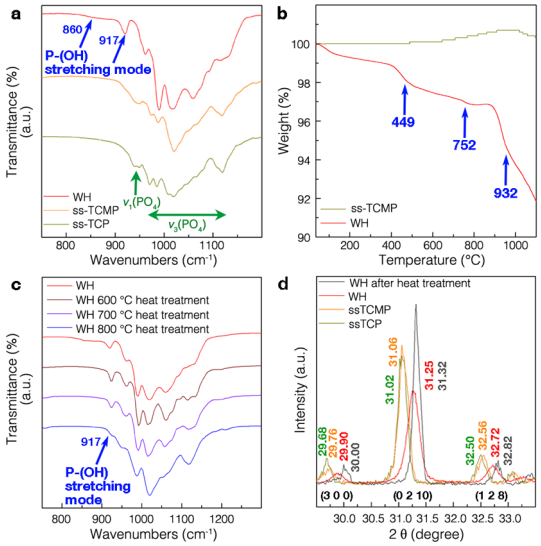

Figure 4. (a) FT-IR analysis result of our synthesized whitlockite (WH: red line), revealing the existence of P−O−H bonds from the HPO_4^{2-} group in its structure. However, the tricalcium phosphate (ss-TCP: green line) and magnesium-substituted tricalcium phosphate (ss-TCMP: yellow line) only contained bonds from PO_4^{3-} without any P−O−H bonds. (b) TGA analysis of WH (red line) revealing a decrease in weight due to the dehydration of the HPO_4^{2-} group. However, no weight decrease was observed in ss-TCMP (green line). (c) FT-IR analysis result demonstrating that the P−O−H bond in WH gradually decreased with increases in the temperature of the heat treatment. (d) XRD analysis of WH (red line), WH after heat treatment at 1450 °C (gray line), ss-TCMP (yellow line), and ss-TCP (green line), demonstrating that the incorporation of Mg^{2+} and HPO_4^{2-} induced shifts of the (3 0 0), (0 2 10), and (1 2 8) peaks toward higher angular positions.

WH in the precipitants decreased. This experiment clearly demonstrated that the WH could precipitate in an acidic environment with the incorporation of Mg^{2+}, which prevented HAP precipitation.

To better understand the mechanism and to obtain pure WH, we focused on the region between $x = 0.1$ and $x = 0.2$. The results indicated that the pure WH phase precipitated when $x = 0.13$, between the WH + DCPA heterogeneous region ($x < 0.125$) and the WH + MP heterogeneous region ($x > 0.135$). According to inductively coupled plasma (ICP) analysis, well-synthesized WH was a stoichiometric compound with a ratio of Ca:Mg:P = 1.27 ± 0.06:0.14 ± 0.02:1, which matches the theoretical ratio (1.28:0.14:1).

In Figure 3a, XRD analysis of our synthesized WH demonstrated that a pure WH phase was formed. We heat-treated the WH at temperatures as high as 1450 °C to verify its high purity. If secondary phases exist in the amorphous state, high-temperature heat treatment can crystallize these phases and make them detectable by XRD. However, no secondary phase appeared after heat treatment at 1450 °C. Therefore, we confirmed that WH was precipitated in a completely homogeneous phase. There was also no indication of a phase change in XRD pattern during heat treatment until WH transformed into the liquid phase at approximately 1600 °C. In addition, as illustrated in Figure 3b and c, our synthesized WH particles were homogeneous, with rhombohedral shapes and sizes of approximately 50 nm. The interplanar distance of the WH nanoparticles was measured to be 8.067 Å by high-resolution transmission electron microscopy (HRTEM) (bottom right inset of Figure 3c), which corresponded well to the *d*-spacing value of the WH (0 1 2) plane (JCDPS No. 70-2064).

To distinguish our synthesized WH from the TCP phase, we provided evidence of the existence of HPO_4^{2-} in the WH structure. As shown in Figure 4a, Fourier transform infrared spectroscopy (FT-IR) analysis demonstrated that P−O−H bonds were present only in the WH compound formed using the precipitation method, while only P−O related bonds were present in the ss-TCP and ss-TCMP prepared using the solid-state method. In addition, we observed that this P−O−H group in the WH structure could be lost during heat treatment by thermogravimetric (TGA) analysis, as shown in Figure 4b. While the initial decrease in the WH weight is caused by the evaporation of water molecules, the subsequent peaks at approximately 449 and 752 °C suggest the transformation of HPO_4^{2-} into $P_2O_7^{4-}$ and PO_4^{3-}.[1,29] The rapid decrease in the WH weight at approximately 932 °C is also a unique phenomenon of WH during heat treatment.[27] After these dehydration processes, WH loses its HPO_4^{2-} group and transforms into the TCP structure.[2,26−28] In contrast, there was no weight change in ss-TCMP during TGA analysis, and a rather slight weight increase occurred due to N_2 gas adsorption on the surface of

the particles. In Figure 4c, we compare the FT-IR results of the WH compounds after being heat treated at different temperatures, and we confirmed that the P−O−H peak disappeared above 800 °C but remained until 700 °C. Therefore, WH can maintain its structural properties below this temperature. In Figure 4d, we carefully compare the XRD peak positions of various TCP, TCMP and WH samples. As the substitution ratio of Mg^{2+} increased from TCP to TCMP (Ca:Mg ≈ 20:1 in mole %) to WH (Ca:Mg ≈ 9:1 in mole %), the lattices contracted and the XRD peaks shifted toward higher angular positions according to Bragg's law. Similarly, when HPO_4^{2-} was lost in WH by heat treatment at 1450 °C, the peaks shifted again to higher angular positions. All these analysis results clearly demonstrate that WH could be distinguished from TCP and TCMP.

To locate the overall precipitation region of WH, we investigated an optimized ratio between $Ca(OH)_2$, $Mg(OH)_2$, and H_3PO_4, starting from the aforementioned location of $Ca(OH)_2$:$Mg(OH)_2$:H_3PO_4 = 37%:13%:50% (in mole %). On the basis of the experimental results, we marked all the possible synthesis regions of pure WH in Figure 5a and also presented them in Figure 1. Other than these conditions, impurities, such as DCPA or MP, can also be precipitated (Figure S1). To be more specific, WH was produced in more acidic pH conditions with excess Mg^{2+} ions present in the environment. Because MP (K'_{MgHPO4} = 0.0011 M at 25 °C) has a lower thermodynamic dissociation constant than DCPA (K'_{CaHPO4} = 0.0020 M at 25 °C),[30] we hypothesize that Mg^{2+} combines with HPO_4^{2-} more competitively than Ca^{2+} and constructs the A column of WH. Thus, a greater amount of Mg^{2+} may be required to combine with HPO_4^{2-} and inhibit calcium phosphate compound nucleation when the anion-to-cation ratio is higher. When this balance between cations and anions is not maintained, other secondary phases, such as DCPA or MP, are immediately produced and form the heterogeneous region.

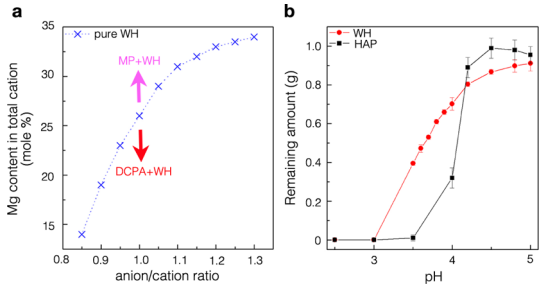

Figure 5. (a) Synthetic conditions of pure whitlockite (WH) from the $Ca(OH)_2$−$Mg(OH)_2$−H_3PO_4 system, which are plotted as blue cross symbols, with the *x*-axis being the ratio of the anion (P) to cations (Ca + Mg) in mole % and the *y*-axis being the content of Mg in the total cation (Ca + Mg), also in mole %. (b) Solubility test of WH and hydroxyapatite (HAP) in the acidic pH region. The remaining amounts of WH and HAP after 24 h of aging in 100 mL of aqueous solution were compared. The initial amount of each powder was 1 g, and the pH was titrated using H_3PO_4 at room temperature.

We also observed stability of WH in various pH regions. The precipitated WH was neutral in distilled water and maintained its homogeneous phase even after aging for 15 days in a 90 °C alkaline environment (0.01 g/mL WH in 100 mL of disodium hydrogen phosphate/sodium hydroxide buffer, pH 12), as demonstrated in Figure S2. In addition, we compared the remaining amounts of WH and HAP after aging 24 h in H_3PO_4 aqueous solutions (0.01 g/mL WH and HAP in 100 mL of a H_3PO_4 aqueous solution from pH 2.5 to pH 5) at room temperature. Notably, as demonstrated in Figure 5b, when the pH decreased from 4.2 to 4.0, the remaining amounts of WH and HAP decreased from 0.804 and 0.89 g to 0.702 and 0.32 g, respectively. These data suggest that WH has higher stability than HAP below pH 4.2. An interesting future issue would be to investigate the correlation between the formation of WH and the acidic environment in our body.[8,31−33] Local areas *in vivo* are often exposed to acidic environments. For example, old and weak parts of the bone are continuously dissolved by acidic chemicals secreted by osteoclast cells, which are estimated to have pH values of 3−4.5.[31−33]

To compare biocompatibility, we grew human osteoblast cells (Lonza Clonetics) on the surface of WH, HAP, and TCP that were all fabricated into cylindrical pellet form. Cells were seeded on the surface of the pellet with a diameter of 1 cm, at a density of 1×10^5 cells/mL. Cell proliferation level on each material (n = 10) was compared by the 3-(4,5-dimethylthiazol-2-yl)-2,5-diphenyltetrazolium bromide (MTT) assay at day 1, day 4, day 7, and day 10 after seeding point (day 0). It is already known that HAP has better biocompatibility than TCP for cell growth,[34] and our result also showed a similar tendency (Figure 6a). Interestingly, cells grown on the WH pellet showed an even better proliferation state than the growth level of cells on the HAP pellet. In addition, as shown in Figure 6b−g, the cell growth state on the surface of each material was directly observed by staining nuclei and the actin cytoskeleton network in cells by DAPI (green) and phalloidin (red), respectively, at day 4 and day 7. Analogous with the MTT result, cells grew vigorously on the whole surface of both WH and HAP. On the contrary, few cells grew on the surface of the TCP pellet.

In addition, to verify that bone cells were not only proliferating on the surface of the WH pellet but also active in the bone formation process, quantified gene expressions associated with the bone-mineralization process were compared relative to HAP, as described in Figure 6h. After 2 days of osteoblast cell growth on the surface of HAP and WH pellet, RNA was extracted from the cells of each sample. Real-time quantitative PCR (RT-qPCR) analysis was conducted to evaluate the mRNA level of cells from each sample (n = 5), and ΔΔCt method was used on the basis of mRNA level of cells grown on the HAP surface. The data from the RT-qPCR

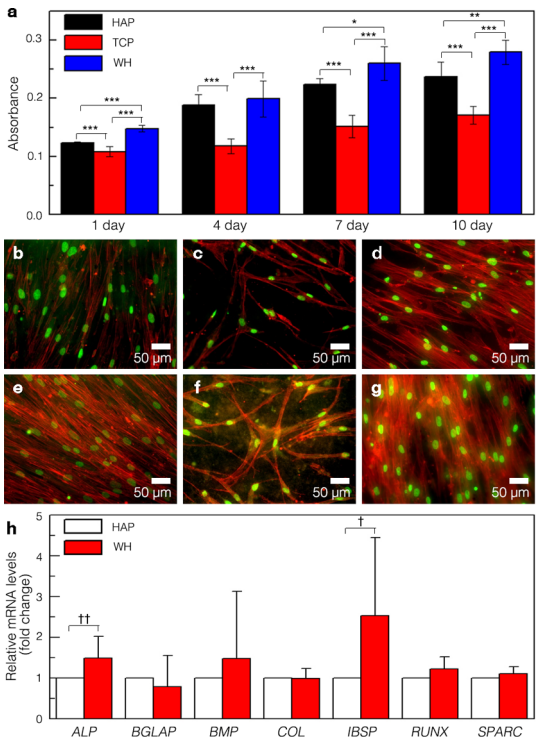

Figure 6. (a) MTT cell proliferation test of human osteoblast cells grown on the surface of hydroxyapatite (HAP, black), tricalcium phosphate (TCP, red), and whitlockite (WH, blue) in cylindrical pellet form. From the initial seeding point (0 day), the amount of cells on each sample was compared after 1, 4, 7, and 10 days ($n = 10$). (b–g) Fluorescence images of cells grown on the surface of a cylindrical pellet made of (b) HAP, (c) TCP, and (d) WH after 4 days and (e) HAP, (f) TCP, and (g) WH after 7 days. Nuclei and the actin cytoskeleton network of cells were stained by DAPI (green) and phalloidin (red), respectively. (h) Relative gene expression evaluated by quantitative real time PCR indicated that osteoblasts grown on WH expressed an equivalent level of bone formation associated genes compared to the cells grown on HAP. The statistical significances between the two groups were determined by Student's *t* test. $^{\dagger}p < 0.1$, $^{\dagger\dagger}p < 0.05$, $*p < 0.01$, $**p < 0.005$, $***p < 0.001$.

analysis showed that WH reinforced osteoblast cell function equivalent to the bone cells grown on HAP.

The growth rate and the gene expression level of the human bone cells grown on the WH scaffold were similar or slightly higher compared to that of HAP and TCP in the current experiment model. However, in addition to the intrinsic property of WH, we notice that better biocompatibility of WH might be induced from many factors such as nanostructure, mechanical hardness, and roughness. Therefore, careful analysis of the exact mechanism can be the next important issue that can be investigated. For example, we found that the Vickers hardness value of the scaffold made from WH was approximately 0.9 GPa, while that of HAP and TCP were about 0.42 and 0.19 GPa, respectively. Additionally, it is possible that Mg incorporation in WH can be one of the enhancing factors, as previously studied in other Mg-doped calcium phosphate systems. Increment of adhesion, proliferation, gene expression related to bone mineralization, and amount of calcium-containing mineral deposition of osteoblast grown on the Mg-doped calcium phosphate compounds have been reported before.[35−38] Although the exact mechanism is still under study, the data presented here suggest a great possibility that can initiate the development and application of WH.

CONCLUSIONS

The approach presented here for the synthesis of pure WH nanoparticles has scientific importance because of the discovery of new precipitation conditions in the ternary $Ca(OH)_2$–$Mg(OH)_2$–H_3PO_4 system and offers technological potential for further applications. Our results demonstrated that pure WH can precipitate under acidic pH conditions. Excess Mg^{2+} in the system also impeded the formation of HAP and other kinetically favored calcium phosphate intermediate phases. Synthesized pure WH nanoparticles showed excellent biocompatibility, which was comparable with HAP and much better than previous bulk TCP. We expect that this study will contribute to the understanding of the precipitation mechanism of calcium phosphate compounds in physiological systems and become a platform for synthesizing technologically important bioceramics.

METHODS

WH was synthesized using a precipitation method with calcium hydroxide ($Ca(OH)_2$, 99.0%, High Purity Chemical, Japan), magnesium hydroxide ($Mg(OH)_2$, 95.0%, Junsei Chemical Co., Japan), and phosphoric acid (H_3PO_4, 85.0%, Junsei Chemical Co., Japan) in a water-based system. Initially, $Ca(OH)_2$ and $Mg(OH)_2$ were mixed at the suggested ratios in Figures 1 and 5a, and heat was applied between 60 and 90 °C to achieve a fast kinetic reaction. Then, according to Figures 1 and 5a, an appropriate amount of H_3PO_4 was added dropwise at a rate of 12.5 mL/min into the $Ca(OH)_2$ and $Mg(OH)_2$ mixed solution using a digital buret (Metrohm 876, Dosimat Plus) while vigorously stirring. The precipitates were aged for more than 9 h and then filter-pressed and dried using a lyophilizer. HAP was also synthesized using a similar precipitation method with identical starting materials. First, 500 mL of a 0.5 M $Ca(OH)_2$ aqueous solution and 500 mL of a 0.3 M H_3PO_4 aqueous solution were prepared. Then, the H_3PO_4 solution was added dropwise at a rate of 12.5 mL/min to the $Ca(OH)_2$ aqueous solution while continuously stirring. After 24 h, the precipitants were filter-pressed to be collected and freeze-dried. TCP ($Ca_3(PO_4)_2$) and TCMP ($Ca_{2.86}Mg_{0.14}(PO_4)_2$) were synthesized using a general solid-state method with calcium carbonate ($CaCO_3$, 99.99%, High Purity Chemical, Japan), magnesium carbonate ($MgCO_3$, 99.9%, High Purity Chemical, Japan), and diammonium hydrogen phosphate ($(NH_4)_2HPO_4$, 99.0%, Junsei Chemical Co., Japan). Each sample was prepared according to its molar ratios and mixed with 1% dispersant in an ethanol solution. The weight ratio between ethanol and the whole powders was 1 to 1. After all the samples

were ball milled for 48 h, the green powders were sintered at 1100 °C for 2 h.

The atomic structure in Figure 2 was drawn using the software CrystalMaker (CrystalMaker Software Ltd., Oxford, England (www.crystalmaker.com)) based on previously reported databases of the crystal structures of WH,[28] TCP,[39] and TCMP.[40] X-ray diffraction (XRD, M18XHF-SRA, MAC Science Co.) with monochromatic Cu Kα radiation (λ = 1.5405 Å) was used to analyze the crystal structure of WH and other reference samples at a scan rate of 1°/min. Field emission scanning electron microscopy (FESEM, JSM-6330F, JEOL) was used to examine the overall morphologies of the WH nanoparticles. To examine the individual shapes of the WH nanoparticles, the WH nanoparticles were dispersed in ethanol and loaded on a copper grid. Then, the WH nanoparticles were observed using high-resolution transmission electron microscopy (HRTEM, JEM-3000F, JEOL), and their *d*-spacing values were also measured. Fourier transform infrared (FT-IR, Nicolet 6700, Thermo Scientific) analysis was conducted to confirm HPO_4^{2-} group existence in WH. Each sample was homogeneously grounded with potassium bromide (KBr) and pelletized to be analyzed in transmission mode. Thermogravimetric analysis (Simultaneous DTA/TGA analyzer, TA Instruments) was performed at temperatures as high as 1100 °C with a 10 °C/min heating rate in a nitrogen atmosphere to examine the dehydration phenomenon of WH. In addition, the ratios of Ca, Mg, and P in the WH samples synthesized from various experimental conditions were analyzed using an inductively coupled plasma optical emission spectrometer (ICP-OES, Varian 720-ES). To test the stability of WH in various pH regions, 1 g of WH was dispersed in 100 mL of distilled water for 1 month. WH was also dispersed in a pH 12 sodium hydrogen phosphate/sodium hydroxide buffer for 15 days at 90 °C. In addition, 1 g of WH and HAP were dispersed in 100 mL of H_3PO_4 aqueous solutions, which were titrated from pH 2.5 to pH 5.0 at room temperature. After 24 h of aging, each remaining powder was collected by centrifuge (13 000 rpm, 10 min) and freeze-dried. Then, the remaining amount of the powder from each condition was measured to compare its solubility. Each sample was subjected to analysis in triplicate.

To compare the biocompatibility of the WH with HAP and TCP, all powders were pressed into cylindrical pellet form with a diameter of 1 cm and heat treated up to 700 °C for 2 h. After sterilization, each pellet was placed in a 24-well plate. Lonza Clonetics human osteoblasts were seeded on the surface of each pellet at a density of 1×10^5 cells/mL (day 0) with Lonza osteoblast basal medium containing fetal bovine serum (FBS), ascorbic acid, and GA-1000. Then, cell-seeded samples were kept in a water-jacketed incubator maintained at 37 °C and 5% CO_2. After 1, 4, 7, and 10 days, pellets with cells growing on its surface were taken out, and each pellet was gently washed with phosphate-buffered saline (PBS, Cellgro, Mediatech. Inc.). Then 20 μL of a 5 mg/mL MTT (thiazolyl blue tetrazolium bromide, Sigma) solution diluted with media (MTT:media = 1:9) was added on the top surface of each pellet. All the samples were kept in the CO_2 incubator for 2 h. After PBS washing, 200 μL of dimethyl sulfoxide (DMSO, Sigma) was added to break the cell membrane. Solution from the each sample was collected, and the absorbance was measured by the multiple plate reader (Victor 3, Perkin-Elmer) at 544 nm. For the cell stained image, after 4 and 7 days, cells grown on the surface of each sample were fixed with 3.7% formaldehyde (Sigma) diluted in PBS for 10 min. Then, the cells were permeabilized with 0.2% Triton X-100 (Sigma) diluted in PBS for 10 min. The actin cytoskeleton network was stained with phalloidin (fluorescein isothiocyanate labeled, Sigma) for 90 min, and then, nuclei were stained with DAPI (4′,6-diamidino-2-phenylindole dihydrochloride, Sigma) for 10 min. After every step, the samples were gently washed with PBS. Finally, the cell proliferation state was observed by fluorescence microscopy (Axio Observer inverted microscope, Carl Zeiss).

Real-time PCR was performed by Rotor Gene Q (Qiagen, Santa Clarita, CA, USA) using the Rotor Gene SYBR green PCR kit. RNA of cells grown on each sample was extracted by an RNA extraction reagent (RNAios Plus, Takara). First-strand cDNA was synthesized from collected RNA with a QuantiTech reverse transcription kit (Qiagen). The following primers from the QuantiTect primer assay (Qiagen) were used: 18S rRNA (*RRN18S*, QT00199367), alkaline phosphatase (*ALP*, QT00012957), bone gamma-carboxyglutamate (*Gla*) protein (*BGLAP*, QT00232771), bone morphogenetic protein 2 (*BMP2*, QT00012544), collagen type I (*COL1*, QT00037793), integrin-binding sialoprotein (*BSP*, QT00093709), runt-related transcription factor 2 (*RUNX2*, QT00020517), and secreted protein acidic cysteine-rich (*SPARC*, QT00018620). To amplify cDNA, the initial activation step was 3 min at 95 °C. Then a denaturation and annealing extension cycle proceeded at 3 s at 95 °C and 10 s at 60 °C, respectively. Differences in gene expression between samples were calculated using the ΔΔCt method. The numbers of samples used for WH and for the control HAP were both $n = 5$, and each sample was analyzed in triplicate. The statistical analyses were performed using SPSS version 21.0. The statistical significances between two groups were compared using Student's *t* test after their normal distribution was confirmed by the Shapiro−Wilk test ($^{\dagger}p < 0.1$, $^{\dagger\dagger}p < 0.05$, $^{*}p < 0.01$, $^{**}p < 0.005$, $^{***}p < 0.001$).

Conflict of Interest: The authors declare no competing financial interest.

Supporting Information Available: A detailed X-ray diffraction analysis and the stability test of WH. This material is available free of charge *via* the Internet at http://pubs.acs.org.

Acknowledgment. This research was supported by the Basic Science Research Program (grant number 2011-0011225), the Global Frontier R&D Program on Center for Multiscale Energy System (grant number 0420-20130104), the Pioneer Research Center Program (grant number 2011-0027888), the Fusion Research Program for Green Technologies (grant number 2012M3C1A1048863), and the International Research & Development Program (grant number 2013K1A3A1A32035536) of the National Research Foundation of Korea (NRF) funded by the Ministry of Science, ICT & Future Planning.

REFERENCES AND NOTES

1. Elliott, J. C. *Structure and Chemistry of the Apatites and Other Calcium Orthophosphates*; Elsevier Science & Technology: Amsterdam, 1994.
2. Driessens, F. C. M.; Verbeeck, R. M. H. *Biominerals*; CRC Press: Boca Raton, FL, 1990.
3. Lagier, R.; Baud, C. A. Magnesium Whitlockite, a Calcium Phosphate Crystal of Special Interest in Pathology. *Pathol. Res. Pract.* **2003**, *199*, 329–335.
4. Scotchford, C. A.; Vickers, M.; Ali, S. Y. The Isolation and Characterization of Magnesium Whitlockite Crystals from Human Articular-Cartilage. *Osteoarthr. Cartil.* **1995**, *3*, 79–94.
5. Hayashi, Y. High-Resolution Electron Microscopy of Mineral Deposits on a Thin Layer of Pellicle Adhering to Intact Enamel Surface. *Electron Microsc.* **1996**, *45*, 501–504.
6. Palamara, J.; Phakey, P. P.; Rachinger, W. A.; Orams, H. J. Electron Microscopy of Surface Enamel of Human Unerupted and Erupted Teeth. *Arch. Oral. Biol.* **1980**, *25*, 715–725.
7. Cashman, K. D.; Flynn, A. Optimal Nutrition: Calcium, Magnesium and Phosphorus. *Proc. Nutr. Soc.* **1999**, *58*, 477–487.
8. Hannig, M.; Hannig, C. Nanomaterials in Preventive Dentistry. *Nat. Nanotechnol.* **2010**, *5*, 565–569.
9. Colfen, H. Biomineralization: A Crystal-Clear View. *Nat. Mater.* **2010**, *9*, 960–961.
10. Jackson, S. F.; Randall, J. T. The Fine Structure of Bone. *Nature* **1956**, *178*, 798–798.
11. Terpstra, R.; Driessens, F. Magnesium in Tooth Enamel and Synthetic Apatites. *Calcif. Tissue Int.* **1986**, *39*, 348–354.
12. Meinke, D. K.; Skinner, H. C. W.; Thomson, K. S. X-Ray Diffraction of the Calcified Tissues in Polypterus. *Calcif. Tissue Int.* **1979**, *28*, 37–42.
13. Quint, P.; Althoff, J.; Hohling, H. J.; Boyde, A.; Laabs, W. A. Characteristic Molar Ratios of Magnesium, Carbon-Dioxide, Calcium and Phosphorus in the Mineralizing Fracture Callus and Predentine. *Calcif. Tissue Int.* **1980**, *32*, 257–261.
14. Koutsoukos, P.; Amjad, Z.; Tomson, M. B.; Nancollas, G. H. Crystallization of Calcium Phosphates. A Constant Composition Study. *J. Am. Chem. Soc.* **1980**, *102*, 1553–1557.

15. LeGeros, R.; Daculsi, G.; Kijkowska, R.; Kerebel, B. *Magnesium in Health and Disease*; John Libbey: New York, 1989.
16. Rowles, S. The Precipitation of Whitlockite from Aqueous Solutions. *Bull. Soc. Chim. Fr.* **1968**, 1797–1802.
17. Ben Abdelkader, S.; Ben Cherifa, A.; Coulet, M.; Khattech, I.; Rogez, J.; Jemal, M. Enthalpie De Formation De La Whitlockite $Ca_{18}Mg_2H_2(PO_4)_{14}$. *J. Therm. Anal. Calorim.* **2004**, *77*, 863–871.
18. Okazaki, M.; Takahashi, J.; Kimura, H. Unstable Behavior of Magnesium Containing Hydroxyapatites. *Caries Res.* **1986**, *20*, 324–331.
19. Ryan, L. M.; Cheung, H. S.; LeGeros, R. Z.; Kurup, I. V.; Toth, J.; Westfall, P. R.; McCarthy, G. M. Cellular Responses to Whitlockite. *Calcif. Tissue Int.* **1999**, *65*, 374–377.
20. Rothwell, W. P.; Waugh, J. S.; Yesinowski, J. P. High-Resolution Variable-Temperature Phosphorus-31 NMR of Solid Calcium Phosphates. *J. Am. Chem. Soc.* **1980**, *102*, 2637–2643.
21. Verbeeck, R. M. H.; De Bruyne, P. A. M.; Driessens, F. C. M.; Terpstra, R. A.; Verbeek, F. Solubility Behaviour of Mg-Containing β-$Ca_3(PO_4)_2$. *Bull. Soc. Chim. Belg.* **1986**, *95*, 455–476.
22. Martens, C. S.; Harriss, R. C. Inhibition of Apatite Precipitation in the Marine Environment by Magnesium Ions. *Geochim. Cosmochim. Acta* **1970**, *34*, 621–625.
23. Nancollas, G.; Tomazic, B.; Tomson, M. The Precipitation of Calcium Phosphates in the Presence of Magnesium. *Croat. Chem. Acta* **1976**, *48*, 431–438.
24. LeGeros, R.; Shirra, W.; Miravite, M.; LeGeros, J. Amorphous Calcium Phosphates: Synthetic and Biological. *Coll. Int. CNRS* **1975**, *230*, 105–115.
25. Trautz, O. R.; Zapantal, R.; Legeros, J. P. Effect of Magnesium on Various Calcium Phosphates. *J. Dent. Res.* **1964**, *43*, 751–754.
26. Gopal, R.; Calvo, C. Structural Relationship of Whitlockite and $\beta Ca_3(PO_4)_2$. *Nat. Phys. Sci.* **1972**, *237*, 30–32.
27. Gopal, R.; Calvo, C.; Ito, J.; Sabine, W. K. Crystal-Structure of Synthetic Mg-Whitlockite, $Ca_{18}Mg_2H_2(PO_4)_{14}$. *Can. J. Chem.* **1974**, *52*, 1155–1164.
28. Calvo, C.; Gopal, R. Crystal-Structure of Whitlockite from Palermo Quarry. *Am. Mineral.* **1975**, *60*, 120–133.
29. Gee, A.; Deitz, V. R. Pyrophosphate Formation upon Ignition of Precipitated Basic Calcium Phosphates. *J. Am. Chem. Soc.* **1955**, *77*, 2961–2965.
30. Walser, M. Ion Association. VI. Interactions between Calcium, Magnesium, Inorganic Phosphate, Citrate and Protein in Normal Human Plasma. *J. Clin. Invest.* **1961**, *40*, 723–730.
31. Ferron, M.; Wei, J.; Yoshizawa, T.; Del Fattore, A.; DePinho, R. A.; Teti, A.; Ducy, P.; Karsenty, G. Insulin Signaling in Osteoblasts Integrates Bone Remodeling and Energy Metabolism. *Cell* **2010**, *142*, 296–308.
32. Teitelbaum, S. L. Bone Resorption by Osteoclasts. *Science* **2000**, *289*, 1504–1508.
33. Silver, I. A.; Murrills, R. J.; Etherington, D. J. Microelectrode Studies on the Acid Microenvironment beneath Adherent Macrophages and Osteoclasts. *Exp. Cell. Res.* **1988**, *175*, 266–276.
34. Jalota, S.; Bhaduri, S. B.; Tas, A. C. In Vitro Testing of Calcium Phosphate (HA, TCP, and Biphasic HA-TCP) Whiskers. *J. Biomed. Mater. Res. Part A* **2006**, *78A*, 481–490.
35. Sader, M. S.; LeGeros, R. Z.; Soares, G. A. Human Osteoblasts Adhesion and Proliferation on Magnesium-Substituted Tricalcium Phosphate Dense Tablets. *J. Mater. Sci. Mater. Med.* **2009**, *20*, 521–527.
36. Webster, T. J.; Ergun, C.; Doremus, R. H.; Bizios, R. Hydroxylapatite with Substituted Magnesium, Zinc, Cadmium, and Yttrium. II. Mechanisms of Osteoblast Adhesion. *J. Biomed. Mater. Res.* **2002**, *59*, 312–317.
37. Bracci, B.; Torricelli, P.; Panzavolta, S.; Boanini, E.; Giardino, R.; Bigi, A. Effect of Mg^{2+}, Sr^{2+}, and Mn^{2+} on the Chemico-Physical and in Vitro Biological Properties of Calcium Phosphate Biomimetic Coatings. *J. Inorg. Biochem.* **2009**, *103*, 1666–1674.
38. Webster, T. J.; Massa-Schlueter, E. A.; Smith, J. L.; Slamovich, E. B. Osteoblast Response to Hydroxyapatite Doped with Divalent and Trivalent Cations. *Biomaterials* **2004**, *25*, 2111–2121.
39. Sugiyama, K.; Tokonami, M. Structure and Crystal Chemistry of a Dense Polymorph of Tricalcium Phosphate $Ca_3(PO_4)_2$: A Host to Accommodate Large Lithophile Elements in the Earth's Mantle. *Phys. Chem. Miner.* **1987**, *15*, 125–130.
40. Schroeder, L.; Dickens, B.; Brown, W. Crystallographic Studies of the Role of Mg as a Stabilizing Impurity in β-$Ca_3(PO_4)_2$. II. Refinement of Mg-Containing β-$Ca_3(PO_4)_2$. *J. Solid State Chem.* **1977**, *22*, 253–262.